THE ROLE OF CARBON NANOTUBES ON THE STABILITY OF TETRAGONAL ZIRCONIA POLYCRYSTALS

A. Morales–Rodríguez[1,2,*], R. Poyato[2], F. Gutiérrez–Mora[1,2], A. Muñoz[1],

A. Gallardo–López[1,2]

[1]Departamento de Física de la Materia Condensada, Universidad de Sevilla, Apdo.1065, 41080 Sevilla, Spain.

[2]Instituto de Ciencia de Materiales de Sevilla, CSIC–Universidad de Sevilla, 41092 Sevilla, Spain.

* Corresponding author. Tel.: +34 954 55 60 28; fax: +34 954 55 28 70. E-mail address: amr@us.es (A. Morales–Rodríguez).

ABSTRACT

The effect of single walled carbon nanotubes (SWNT) at zirconia grain boundaries on the stability of a tetragonal zirconia polycrystalline matrix has been explored in as–sintered composites and after low–temperature hydrothermal degradation (LTD) experiments. For this purpose, highly–dense 3 mol% Y_2O_3–doped tetragonal polycrystalline (3YTZP) ceramics and SWNT/3YTZP composites were prepared by spark plasma sintering (SPS). Quantitative X–ray diffraction analysis and microstructural observations point out that an increasing amount of well–dispersed SWNT bundles surrounding zirconia grains decreases the metastable tetragonal phase retention in the ceramic matrix after sintering. In contrast, the tetragonal ceramic grains in composites with SWNTs are less sensitive to the presence of water, i.e. to undergo a martensitic transformation under LTD conditions, than monolithic 3YTZP ceramics. The SWNT incorporation diminishes micro–cracking due to tetragonal to monoclinic ZrO_2 phase transformation in the composites.

Keywords: ZrO_2; Carbon nanotubes; Phase transformation; LTD

1. INTRODUCTION

Yttria–stabilized tetragonal zirconia polycrystalline (Y–TZP) ceramics offer an attractive combination of strength, fracture toughness, ionic conductivity and low thermal conductivity making them ideal candidates for high–performance in a wide variety of fields ranging from bearings with high wear resistance, solid oxide fuel cell applications to biomedical devices [1]. By alloying with Y_2O_3, as with other aliovalent ions, the large concentration of oxygen vacancies introduced in the lattice can stabilize the high–temperature ZrO_2 crystallographic phases (tetragonal and cubic phases) at room temperature by avoiding the tetragonal to monoclinic transformation during cooling from sintering temperature. The key point for the high fracture toughness exhibited by these ceramics is that the metastable tetragonal phase retained down to room temperature undergoes transformation to monoclinic phase during crack propagation [2], acting as the main mechanism responsible for the toughening increase.

The major drawback of Y–TZP is that these ceramics are prone to aging, meaning that metastable tetragonal grains are very susceptible to slowly transform to monoclinic phase triggered by water–derived species [1]. This transformation entails surface roughening and micro–cracking which lead to degradation of the attractive mechanical properties of tetragonal zirconia. Different strategies developed for the increase of Y–TZP aging resistance involve reducing the tetragonal to monoclinic transformability of the zirconia, for instance, by grain size refinement to submicrometric level. However, achieving a more stable tetragonal phase delays aging but it also implies less transformability under stress and therefore the loss of the ability of transformation toughening, which diminishes the resistance to crack propagation [3].

Many parameters influence the transformability of Y-TZP ceramics such as grain size and morphology, grain boundary phase, and yttria content and distribution. Fracture toughness in the Y-TZP system strongly depends on the grain size and amount of yttria content. Several authors have observed that the fracture toughness increases with grain size after annealing Y-TZP samples [4,5]. Performing post-sintering heat treatments at different temperatures on 3Y-TZP samples, Ruiz and Ready [4] found that the fracture toughness increased from 4 to 10 $MPa \cdot m^{1/2}$ with grain size increasing from 1 to 10 μm. The yttria content also influences the transformation toughening but, in general, in the opposite sense, i.e. toughness increases with decreasing yttria content. For yttria contents lower than 2 mol%, the Y-TZP ceramics exhibit high indentation toughness values (> 10 MPa $m^{1/2}$) [6 -10]. Indentation toughness up to 14 MPa has been reported for 1.5Y-TZP ceramics

[10]. The wetting of zirconia grains by a thin glassy phase has also an enhancing effect on the toughness of TZPs [11]. Zhan et al. [12] have recently shown that grain-boundary segregation of certain trivalent cations significantly improve the hydrothermal aging instability of yttria-based zirconia ceramics. The authors claimed that changing grain-boundary features provides a promising approach to improve aging and crack propagation resistance in Y-TZP ceramics [12].

Incorporating secondary phases with high tensile strength and stiffness, nanoscale flexibility and low density into a ceramic matrix has become an interesting field of study during the last decades to overcome their deficient fracture toughness. In this sense, great attention has been paid to composites with carbon nanotubes (CNTs).

Padture [13] pointed out that these ceramic composites possess unique grain–boundaries structures containing a 2D tangled net of tortuous 1D CNTs extended as a 3D throughout the composite. Since these reinforcing structures are nanometric, flexible and entangled within the ceramic grain microstructure, they provide a non–classical toughening mechanism of uncoiling and stretching: intergranular crack advance leads to uncoiling of the carbon nanotubes and, with further crack propagation, they stretch bridging the crack as both their ends are anchored to the grain boundary [13]. This toughening mechanism opens the possibility of tailoring CNTs–ceramic composites joining both high toughness and high strength, uncommon combination in ceramic–based materials [13].

Regarding the stability of the zirconia crystalline phases, the influence of carbon nanostructures on the zirconia phase structure has been studied in recent years [14–17]. Rani et al. [15] demonstrated that graphene incorporation in fine powders of pure ZrO_2 clearly favours the tetragonal to monoclinic transformation. The dominance of the monoclinic phase compared to the tetragonal or cubic phases increases in the ZrO_2 matrix with increasing graphene content [15]. It is interesting to note that this trend is 54 the opposite to that observed when incorporating carbon atoms to a zirconium oxide structure [18,19]. By carburizing zirconia ceramics embedded into graphite powders at temperatures above 1200 ºC, C atoms can enter the ZrO_2 lattice, stabilizing the high– temperature phases [19]. Several authors also demonstrated by X–ray diffraction (XRD) studies that the presence of carbon nanotubes affects the tetragonal to monoclinic phase transformation that takes place in the zirconia matrix during cooling from sintering temperature [16,17,20]. Poyato et al. [16] showed a noticeably increase of the monoclinic zirconia phase when increasing single walled carbon nanotube content from 2.5 to 10 vol% in 3YTZP

composites. Bocanegra–Bernal et al. [17] have also evidenced such phase transformation induced by the presence of multiwall carbon nanotubes (MWNTs) and graphite powder in 0.01 wt% MWNT/zirconia toughened alumina composites sintered in air. The authors noticed that the phase transformation did not take place when composites were sintered under an argon atmosphere [17]. In the same regard, Kasperski et al. [21] consolidated 3YTZP with double–walled CNTs (DWCNTs) in SPS under a flowing argon atmosphere finding only tetragonal zirconia both in monolithic 3YTZP ceramic and in composites. A plausible explanation for these findings has not been found yet. In this context, further research to give deeper insights on the zirconia stabilization mechanisms in the presence of carbon nanostructures avoiding tetragonal to monoclinic transformation during cooling from sintering temperature is needed. It should be noted that the stabilization of the tetragonal zirconia phase is a multi-factorial issue, and it may depend on CNT dispersion quality but also on sintering conditions such as dwell time, temperature, etc. that may have effect on the carbon diffusion into the zirconia grains or on the zirconia reduction grade which may also influence the transformability of the tetragonal phase.

Controversial results with respect to the effect of CNTs on the martensitic transformation toughening have been reported [22–26]. Zhou et al. [22] claimed that MWCNTs promote the martensitic transformation during crack propagation based on the idea that carbon nanotubes lower the matrix constraint, which remains sufficiently rigid to retain sub–stabilized tetragonal grains, but less compact to easily transform into monoclinic phase. A similar tendency for phase transformation triggered by stress was observed in CNT/3YTZP composites with CNT content above 3 vol%, while the opposite trend was observed in composites with lower contents [25]. By comparing monoclinic content in sintered and crushed 3YTZP with and without MWNTs, Mohapatra et al. [26] found that the tetragonal to monoclinic phase transformation is restricted in 3YTZP with MWNTs. Contrarily to Zhou et al. [22], these authors argued that MWNTs lower the extent of stress–induced transformation by redistributing the applied stress among them, thus decreasing the amount of stress available for phase transformation to metastable tetragonal zirconia crystals [26]. The lower proneness to undergo the phase transformation during crack propagation in composites with higher amount of CNTs has also been attributed to their smaller matrix grain size [23,24,27].

To date, published studies on the influence of carbon nanotubes in the zirconia resistance to hydrothermal degradation after water exposure are scarce. Moisture–driven tetragonal to monoclinic phase transformation seems to be strongly restricted in spark plasma sintered 3YTZP with and without MWCNTs thanks to the microstructure refinement [3]. These authors claimed that the addition of MWCNT appears to

properly balance ageing and crack resistance. Interestingly, the loss of transformation toughening of Y–TZP is compensated in these composites by CNT toughening mechanisms (bridging and CNT pull–out) [3]. The role played by the presence of carbon nanotubes inhibiting the low–temperature degradation is still unclear.

The present study is devoted to understand the role of single walled carbon nanotubes on the tetragonal to monoclinic transformation of 3YTZP ceramics during cooling from sintering temperature. A set of SWNT/3YTZP composites keeping the same grain size with a gradual increase in the SWNT content at grain boundaries has been sintered to assess the influence of the amount and distribution of carbon nanotubes on the 3YTZP ceramic matrix crystalline phases. The as–sintered SWNT/3YTZP composites crystalline phase structure has been investigated by quantitative X–ray diffraction (XRD) studies. Additionally, the aging sensitivity of SWNT/3YTZP composites with 0.5 and 2.5 vol% SWNT compared to the monolithic 3YTZP ceramic has also been tested to check the intrinsic effect of the carbon nanotubes incorporation in the low–temperature degradation process.

2. EXPERIMENTAL

2.1 Raw materials

Monolithic 3YTZP ceramic and SWNT/3YTZP composites with different carbon nanotube nominal content (0.5, 1.5 and 2.5 vol% SWNT) were prepared from commercially available 3YTZP powders with 40 nm average particle size and 99% purity (Nanostructured and Amorphous Materials Inc., Houston, TX) and purified SWNTs with 0.5–1.5 μm typical bundle length and 4–5 nm diameter (Carbon Solutions Inc., Riverside, CA). Commercial SWNTs were functionalized using a mixture of concentrated sulfuric acid (98%) and nitric acid (70%) in a 3:1 volume ratio to disentangle and cut the raw SWNT ropes, as described elsewhere [28]. The raw SWNTs were suspended in this acid mixture for 24 h at room temperature and the suspension was sonicated in low–power ultrasonic bath for 8 h. The COOH–functionalized SWNTs were collected on ~ 20 nm pore alumina filter membranes, washed in high purity ethanol for several times and freeze–dried in order to avoid re–agglomeration. The carboxyl groups introduced on the walls and ends of SWNTs enable their further dispersion in the basic medium used in colloidal processing.

2.2 Processing and sintering

Colloidal processing of the composite powders was carried out in an aqueous solution using ammonia to adjust the solution's pH to 12. Functionalized SWNT suspensions were dispersed by two different sonication procedures to explore the effect of SWNT dispersion degree on the matrix crystallographic phases. On the one hand, some suspensions were dispersed using a high–power ultrasonic probe (~ 750 W) (model KT–600, Kontes Inc., NJ) and, on the other hand, other suspensions using a low–power ultrasonic bath (~ 250 W) (Sonorex digitec DT 255/H, BANDELIN electronic GmbH & Co. KG, Berlín). A fraction of the SWNTs remained in agglomerates in these last suspensions [29].

In a first step, two independent SWNT and ceramic powder (both negatively surface charged) solutions were prepared. The SWNT suspensions were subjected to ultrasonication for 15 min when using a high–power ultrasonic probe or for 30 min when using a low–power ultrasonic bath, respectively. In a second step, both solutions (as–dispersed SWNT and ceramic powder) were mixed in aqueous solution and similarly subjected to ultrasonication by means of the probe (5 min) or the bath (30 min), as appropriate. Hereinafter, samples will be referred to as ultrasonic bath (UB) or ultrasonic probe (UP) according to the dispersion routine followed in each case. Samples will be named indicating their SWNT nominal content followed by UB or UP script as appropriate.

Composite powder blends were dried on a hot plate assisted by stirring, while pH and homogeneity were controlled during the drying process. Finally, composite powders were homogenized in an agate mortar.

The sintering processes were carried out by using a SPS equipment (model 515S, SPS Dr Sinter Inc., Kanagawa, Japan). 15 mm–diameter samples were sintered under vacuum in a cylindrical graphite die/punch setup, under a uniaxial pressure of 75 MPa at 1250 ºC for 5 min. The temperature was measured by means of an optical pyrometer focused on the side of the graphite die. The heating and cooling rates were 300 and 50 ºC/min, respectively. A sheet of graphite paper was placed between the powders and die/punches for easy specimen removal. The as–sintered materials, ~ 3 mm in thickness, were carefully ground up to 1200P SiC sandpaper to eliminate the residual surface graphite.

Bulk densities were measured by Archimedes' method using distilled water as immersion medium. Theoretical density for composites was calculated by the rule of mixtures from density values of 6.10 g cm^{-3} for 3YTZP and 1.80 g cm^{-3} for SWNTs.

2.3 Microstructural and electrical characterization

The structural integrity of the SWNTs in the composites after SPS process was assessed by Raman spectroscopy on fracture surfaces using a dispersive microscope (Horiba Jobin Yvon LabRamHR800, Kyoto, Japan), with a 20–mW He–Ne green laser (532.14 nm), without filter, and with a 600 g/mm grating. The microscope used a 100x objective and a confocal pinhole of 100 □m. The Raman spectrometer was calibrated using a silicon wafer.

High–resolution scanning electron microscopy (HR–SEM) study, using a Hitachi S5200 microscope (Hitachi High–Technologies America Inc., USA), was performed to characterize the morphology of ceramic grains. To reveal grain boundaries, the samples were polished up to 1 μm diamond paste and further thermally etched at 1200 ºC for 20 min in air. Grain size distributions (mean equivalent planar diameter with their standard 54 deviations) were analyzed using *ImageJ* software. Low–magnification conventional SEM (model JEOL 6460LV, JEOL USA Inc., MA, USA) was carried out to check the homogeneity of the carbon nanotubes dispersion from direct observation of the existence or absence of agglomerates in the zirconia matrices.

The influence of the SWNT amount and distribution on the structural phases of the 3YTZP matrix was analyzed by means of XRD measurements in a Bruker D8 Advance A25 diffractometer (Bruker Co, Germany) in Bragg–Brentano configuration. The used detector was a Lynxeye PSD (Bruker, Germany) with a 0.5º fix slit in the incident beam and axial Soller slits of 2.5º in the incident and diffracted beams for copper K_α radiation. Measurements were taken in a wide range of 2θ diffraction angles between 10º and 120º, with a step of 0.015º and a time per step of 0.5 s in order to carry out a quantitative phase Rietveld analysis. The selected experimental conditions allowed registering the intensity of a large number of reflection peaks as well as a large number of counts for each diffraction peak as required to carry out a robust quantitative analysis [30,31]. TOPAS 5 software (Bruker) [32] was used to accurately quantify the wt% of the different crystallographic phases present in the zirconia matrices by Rietveld refinement [31]. Zero error peak shift (2θ), absorption (1/cm) and lattice

parameters of the phases along with no–special sites in tetragonal and monoclinic structures were allowed to vary to provide the best fitting. The background was fitted by a fourth–order Chebyshev polynomial. Correction for preferred orientation effects using an eighth–order spherical harmonics series was also considered in cubic and tetragonal phase refinements. Geometric factors were used for the measurements configuration.

The electrical conductivity at room temperature was obtained by Impedance Spectroscopy using an Agilent 4294A analyzer (Agilent Technologies, US) which operated in a 200 to 2×10^6 Hz frequency range. Colloidal silver paste was applied on two parallel faces of the composites and the samples with the electrodes were fired at 600 ºC for 30 min in Ar flow. The impedance data were analyzed using an equivalent circuit model by means of Z–view software.

2.4 Low–temperature hydrothermal degradation tests

Aging experiments were carried out by keeping polished samples (up to 1 μm diamond 54 paste) in a hydrothermal reactor with a small amount of distilled water at 134 ºC (temperature specified for the LTD tests in the ISO Standards for biocompatible Y-TZP [33]) for different times (1, 4, 10, 24 and 50 hours) to assess the aging sensitivity of the composites. These accelerated LTD experiments were conducted on the monolithic 3YTZP ceramic and the C0.5–UP composite to clarify the effect of the carbon nanotubes incorporation on the aging resistance in the presence of moisture. A 10 h aging test was also carried out on the C2.5–UP composite to check the effect of higher SWNT content on the aging response. This 10 h aging condition was selected expecting a detectable change in the monoclinic fraction in view neither that after 10 h aging tests nor the 3YTZP ceramic nor the C0.5–UP composite have transformed completely monoclinic.

Each sample was examined by XRD before and after aging. The weight fraction of monoclinic zirconia phase was quantified by Rietveld refinement from collected XRD patterns on a diamond polished surface of the samples.

The depth of the monoclinic transformation has been estimated from the micro–cracked layer associated to the propagation of the transformation from surface to the bulk. The micro–cracked zone was observed by SEM inspection of polished cross–sections, perpendicular to the water exposed surface, of samples after 10 h hydrothermal degradation tests.

3. RESULTS

3.1 Microstructure and phase composition of the SWNT/3YTZP composites

Highly–dense SWNT/3YTZP composites were sintered with a similar ceramic grain microstructure regardless the SWNT content and dispersion routines. The microstructural features of these composites are summarized in table I. The electrical conductivity data have been also included in table I as a parameter to estimate electrical percolation of the SWNT network. Mean grain sizes ~ 230 nm were measured in all the as–sintered materials, including the monolithic 3YTZP ceramic. This is in contrast with previous works, as a grain size refinement when increasing CNT content has been reported for 3YTZP/CNT composites [3,23,25,27]. However, it should be noted that, although these authors used ceramic powders with a particle size similar to the one used in the present study, they used MWNT instead of SWNT, and different composite powder processing techniques. Also, differences in terms of SPS conditions are found as they used lower dwell time [3,23,25], temperature [3] or applied pressure [23,25,27].

Raman spectra confirmed the prevalence of undamaged SWNTs in all the composites after SPS as previously shown [20,34]. SEM observations in BSE (backscattered electrons) mode revealed the presence and distribution of SWNTs (dark contrast) dispersed within the 3YTZP ceramic matrix (light contrast) (figures 1A and 1B). The SWNTs are homogeneously distributed at grain boundaries in UP–composites. The ceramic grains are surrounded by SWNTs as shown by the presence of dark contrast around small light areas (figure 1A). HRSEM inspection of fractured surfaces corroborates the excellent dispersion of the SWNT bundles throughout the ceramic matrix (figure 1B). In addition to removing agglomeration, the use of the ultrasonic probe makes the SWNT bundles thinner [20]. In the case of the UB–composites, a fraction of the SWNT content remains in agglomerates (figure 1C) coexisting with agglomerate–free areas where SWNT bundles are surrounding the matrix grains (figure 1D). The main difference between C1.5–UP and C1.5–UB is precisely the degree of SWNT dispersion; while figure 1C shows some agglomerates, the presence of thick bundles in figure 1A is lower and with much smaller size, indicating a better SWNT dispersion and therefore increased homogeneity. The fact that part of the carbon nanotube content is forming agglomerates implies a smaller presence of them at grain boundaries as it can be easily appreciated by comparing the amount of SWNTs on the fracture surfaces (figures 1B and 1D) and data in table I, where the carbon nanotube content at grain boundaries (GB–SWNTs) is

presented. Thanks to the use of two different dispersion routines, a set of samples with a gradual increase in the SWNT content at grain boundaries was available.

Figure 2 presents the XRD patterns corresponding to the polished surfaces of the as–sintered SWNT/3YTZP composites, together with the patterns of the ceramic powders and the monolithic 3YTZP ceramic sintered under the same conditions than the composites (included for comparison). In all samples, the tetragonal phase (JCPDS 01–078–1808) is the main one along with a variable contribution of the monoclinic (JCPDS 01–078–1807) and cubic (JCPDS 00–049–1642) phases. The main peak (1 1 1) corresponding to c–ZrO_2 phase (at $2\theta = 29.9^{o}$) overlaps with the main tetragonal one (1 0 1), widening this t–ZrO_2 peak slightly to the left. According to the diffractograms shown in figure 2A, it can be observed that after sintering this shoulder at lower 2θ values in the tetragonal (1 0 1) reflection is more pronounced in most composites than in the monolithic ceramic pattern. Two intense peaks at 2θ values 28.2 and 31.4º corresponding to monoclinic zirconia (m–ZrO_2), namely (-1 1 1) and (1 1 1) reflections, can be observed in the XRD pattern of the 3YTZP powder. These peaks, clearly visible in the powders' XRD pattern, practically disappear after sintering during 5 min at 1250 ºC (figure 2B).

Focusing on the effect of SWNTs in the sintered composites, it is noted that the incorporation of carbon nanotubes favors the presence of a monoclinic (-1 1 1) peak as shown in figure 2B for the composite C0.5–UP. This peak is not observed in the monolithic 3YTZP nor in the C0.5–UB composite, while it slightly increases for the composites with increasing SWNT content at grain boundaries (figure 2A). This result is in agreement with the clear increase of the two main peaks corresponding to the monoclinic phase reported for higher SWNT content 3YTZP composites (C5–UB and C10–UB) [16]. However, the development of the monoclinic peaks in the X–ray diffractograms of the composites with higher SWNT amount was more remarkable than in the current study. It should be noted that the observed trend agrees between studies, since the monoclinic peaks are gradually increasing with carbon nanotube content from low (0.5 vol%) to high SWNT content (10 vol%). It is also noteworthy that the presence of a higher monoclinic zirconia content does not compromise the microstructural integrity of the as–sintered composites, with no observed micro–cracking damage.

The amount of cubic, tetragonal and monoclinic ZrO_2 phases present in the as–sintered samples was evaluated by Rietveld fitting of the acquired XRD patterns (shown in figure 2). The weight fractions of the different zirconia phases may be certainly inferred from a detailed

analysis of the XRD patterns. Figure 3 shows a zoomed–in view of the experimentally recorded (black line) XRD pattern for the monolithic 3YTZP ceramic in a 2θ–range between 28 and 32º to illustrate the goodness of the Rietveld fitting profiles achieved in this study. In this figure, the main monoclinic, cubic and tetragonal ZrO_2 peaks are identifiable and the calculated profile patterns show a good match with the experimental ones. The best Rietveld fit includes the contribution of 9.3 wt% cubic (red line), 86.0 wt% tetragonal (green line) and 4.8 wt% monoclinic zirconia (blue line) reflection peaks. Reliable fittings require the value of the GOF parameter ("Goodness of fit") to be greater than 1, and as close as possible to it, and the residual factors (R_{wp} and R_{Bragg}) with the smallest possible value for the used measurement configuration [31]. In our analysis, acceptable fitting indicators were obtained (GOF ~ 2–3, R_{wp} ~ 5–7 and R_{Bragg} ~ 1–2, shown in table II). The weight percentages corresponding to cubic, tetragonal and monoclinic ZrO_2 crystallographic phases obtained from the fits are collected in table II. The phase quantities estimated for C5–UB and C10–UB by Rietveld refinement from the X-ray diffractograms published in [16] have also been included.

The c–ZrO_2 phase content in the as–sintered materials is higher than in the 3YTZP powder, despite the low sintering temperature and short time used in SPS. For carbon–containing zirconia ceramics, it has been claimed that both the presence of carbon atoms in the ZrO_2 lattice as well as the nanometer–size of zirconia particles favor the stabilization of the cubic zirconia phase at low temperature [14,19]. The c–ZrO_2 phase content in the as–sintered composites results slightly higher than in the monolithic 3YTZP ceramic, probably due to C diffusion from SWNTs present in the matrix along with a contribution from the SPS graphite mold.

Focusing on the monoclinic content, a greater amount of monoclinic zirconia is found in most of the composites when compared to the monolithic ceramic. Moreover, the monoclinic content clearly increases with increasing well–dispersed SWNTs at ceramic grain boundaries in the composites with SWNT content above a minimum amount of 0.5 GB–SWNT vol%. Figure 4 displays the monoclinic zirconia wt% as a function of the grain–boundary SWNT content for an easier visualization of how well–dispersed carbon nanotubes influence the monoclinic phase content in the composites. An increasing amount of monoclinic weight fraction is found in the composites with increasing GB–SWNT content. A similar m–ZrO_2 percentage has been measured both in C0.5–UB composite and monolithic 3YTZP. Once the amount of carbon nanotubes at grain boundaries is about 0.5–1.1 vol%, a greater amount of monoclinic phase can be clearly detected compared to the value found in the monolithic ceramic. This difference is more noticeable when the GB–SWNT content increases above 2.5 vol%, as it can be

easily seen comparing the quantities of monoclinic phase estimated for the C5–UB and C10–UB composites (table II). Since the processing routine is the main factor concerning SWNT agglomeration, we can assume for the C5–UB and C10–UB GB– SWNT contents the values estimated for SWNT/alumina composites with 5 and 10 SWNT vol% [35] prepared using identical dispersion routine [16]. It should also be noted that the m–ZrO_2 amount in the UB–composites is slightly smaller than the trend shown by the UP–composites.

3.2 Low–temperature hydrothermal degradation of SWNT/3YTZP composites

Figure 5 displays the percentage of monoclinic phase in surface as a function of the hydrothermal aging time for the C0.5–UP composite compared to the monolithic 3YTZP ceramic, both samples with similar ceramic grain size (table I) and containing similar amounts of monoclinic phase before the hydrothermal aging experiments. Data for C2.5–UP composite after 10 and 50 h aging times are also included to roughly compare the aging kinetics with increasing SWNT amount.

For aging times up to 4 h, both the C0.5–UP composite and the 3YTZP ceramic showed almost no evidence of aging, but after 10 h in the hydrothermal reactor, the tetragonal to monoclinic transformation becomes noticeable in the case of the monolithic 3YTZP ceramic. The presence of only 0.5 vol% GB–SWNT homogeneously distributed at ceramic grain boundaries drastically reduces the aging kinetics in the C0.5–UP composite compared to the monolithic ceramic, since up to 50 h in the hydrothermal reactor, the C0.5–UP composite developed less monoclinic phase. A monoclinic–phase saturation level was reached by the monolithic 3YTZP after 24 h of hydrothermal testing, while samples containing SWNT remained under saturation after similar testing times. The comparison of surface transformation curves for the C0.5–UP composite and the 3YTZP monolithic ceramic suggests that the presence of SWNTs at ceramic grain boundaries slows down the martensitic transformation by moisture. Mohamed et al. [38] also found a decrease in the monoclinic content in 3YTZP/MWNT composites compared to the monolithic 3YTZP ceramic after aging for 20 h. However, the 3YTZP low–temperature degradation of composites with MWNT addition [38] decreased in a stronger way than with SWNT addition.

When comparing the effect of increasing GB–SWNT content on aging resistance, it should be taken into account that SWNT/3YTZP composites with higher SWNT content have a greater amount of monoclinic phase after sintering. However, the aging response of the C2.5–

UP composite agrees with the previously mentioned trend (figure 5), the surface t–m transformation slightly increases comparing the monoclinic amount after 10 and 50 h in autoclave pointing out the effect of higher content of carbon nanotubes at grain boundaries on aging kinetics slowdown.

The depth of the micro–cracked layer developed in monolithic 3YTZP after 10 h–aging can be observed in figure 6. The large amount of intergranular fracture associated with the aging degradation is easily observed in SEM by BSE mode inspection as the micro–cracks are filled by the epoxy resin used for embedding the sample to allow polishing preparation without lost of the damaged zone. The cross–section of the monolithic ceramic after aging showed a clear boundary between the micro–cracked zone and the pristine one that allows measuring the extension of the micro–cracked region (about 6–8 μm depth). Nevertheless, the micro–cracked zone is not observed in the cross–sections of the composites after aging. A pristine matrix without any relevant feature is observed in the polished cross–sections of both composites (not shown). Therefore, the monoclinic transformation is much less extensive in the composites, where the damaged zone is undeveloped, and so the aged region is restricted to a region very close to the surface exposed to water.

4. DISCUSSION

The current set of results directly evidences that SWNT incorporation between 3YTZP ceramic grains results in effectively promoting the monoclinic transformation of metastable tetragonal zirconia grains during cooling after SPS consolidation from a threshold amount of carbon nanotubes surrounding ceramic grains (≥0.5 vol% GB–SWNT). In the composites with 0.5 and 1.1 vol% GB–SWNT content, the SWNT network is close to the percolation limit since in this range there is a transition from insulator to electrically conductor behaviour with very low conductivity (see table I). The existence of interconnected (or close to interconnected) GB–SWNTs seems to be the key point in promoting the monoclinic transformation of metastable tetragonal zirconia grains during SPS cooling stage instead of retaining their metastable tetragonal structure to room temperature. In fact, the relation between the monoclinic phase content in the as–sintered composites and the degree of GB–SWNT interconnection also explains the similar monoclinic content presented by the C0.5–UP and C1.5–UB composites despite their different GB–SWNT contents. Taking into account that the thickness of the SWNT bundles is wider in the UB–composites than in the UP–ones [20], for similar GB–SWNT content, logically, thicker bundles of UB–composites are less interconnected

in length than narrower bundles of UP–composites, therefore resulting in a larger amount of metastable tetragonal phase retained in the UB–composites. Once the amount of carbon nanotubes at grain boundaries is high enough to be surrounding many 3YTZP domains by interconnected SWNT paths, these percolated SWNT bundles networks raise the monoclinic zirconia content in electrically conductor composites (starting from C2.5–UP). More interconnected SWNT bundles well–distributed surrounding 3YTZP grains increase both composite conductivity and monoclinic ZrO_2 content after sintering.

To summarize, XRD results correlated to microstructural evidence point out that the presence of well–dispersed GB–SWNTs among ceramic grains disfavours the retention of the zirconia tetragonal phase to room temperature. Besides, the tetragonal to monoclinic transformation that takes place during cooling from the sintering temperature seems to be affected by the percolation degree of the SWNT bundles network. In fact, GB–SWNT percolation has control over the monoclinic zirconia content in as–sintered composites, so that higher monoclinic content is present in composites which show higher electrical conductivity (i.e., with higher percolated SWNT network).

For dense polycrystalline zirconia ceramics, the stabilization of the tetragonal phase is largely dependent on the mutual elastic constraint provided by the neighbouring grains [1]. As the t–m martensitic transformation is accompanied by a volume increase, this transformation is mechanically constrained by the surrounding untransformed 3YTZP grains. When the tetragonal phase is retained, the transformation is mechanically constrained under metastable conditions. This mechanical constraint is directly related to the surrounding matrix elastic modulus and it is also influenced by internal stresses, so that a stiffer matrix and the existence of hydrostatic pressure both favour the retention of the tetragonal phase [1]. In our composites, 3YTZP domains surrounded by the more interconnected SWNT bundle paths could be more likely to transform from tetragonal to monoclinic during cooling from sintering temperature due to lack of enough elastic constraint provided by the neighbouring ceramic grains in these areas. A percolated network of SWNT bundles in a 3YTZP matrix results in composites with regions near the carbon nanotubes that could be more inclined to transform their tetragonal grains into monoclinic phase after SPS consolidation due to looseness among zirconia grains in these regions. The presence of SWNT bundles, when surrounding zirconia domains, relax the mutual elastic constraint that could be exerted by the neighbouring 3YTZP grains, and therefore, lessen the retention of the tetragonal phase to room temperature. For the case of zirconia grains far away from the carbon nanotubes, the constraints among grains could be rigid enough to retain the metastable tetragonal phase during SPS cooling.

Evidence supporting the high capability of CNTs to accommodate stresses in 3YTZP composites has been recently provided by Mohapatra et al. [26] investigating the transformation toughening in zirconia/MWNT composites. Phase analysis of sintered and crushed pellets indicated a significant decrease in the stress–induced phase transformation in the crushed samples of partially stabilized zirconia. By TEM inspection of crushed MWNT–containing 3YTZP samples, which means that the t–m transformation was triggered by a propagating crack, the authors showed that the tetragonal phase was retained in regions near MWNTs whereas the monoclinic phase predominated in regions away from MWNTs. This observation demonstrates that carbon nanotubes do not transfer the applied stress to the matrix, avoiding the martensitic transformation toughening in regions near them when a crack propagates. In this context, it should be noted that the composites of our study showed no cracks after the SPS process, neither the composites with high SWNT content (C10–UB) [16] despite their abundant amount of monoclinic phase present while the usual effect of great amount of monoclinic is cracking. The microstructural integrity observed in C5– 50 UB and C10–UB composites after sintering could be attributed to the presence of SWNT bundles at grain boundaries. SWNTs are extraordinary resilient nanostructures, highly flexible with radial softness [36] and when forming bundles, they easily glide by inter–bundle slippage [37]. In 3YTZP/SWNT composites, GB–SWNT bundles can easily accommodate shear deformation and volume changes associated to t– to m–ZrO_2 phase transformation avoiding the extensive cracking usual in zirconia polycrystalline ceramics when this martensitic transformation occurs during cooling.

According to our results, the single–walled carbon nanotubes at grain boundaries are very effective avoiding micro–cracking. Also, the discontinuity of zirconia grains structure in the composites is expected to block the pathway for diffusion of water–derived species into the ceramic, which implies that the transformation of tetragonal to monoclinic zirconia by moisture find obstacles to evolve to depths beyond the surface either. Therefore, the tetragonal–monoclinic transformation during hydrothermal degradation is strongly restricted in SWNT/3YTZP composites due to the combination of these two effects of the SWNT bundle network, which seems to be very effective limiting transformation propagation from surface to the bulk and so slowing down kinetics for LTD degradation.

Garmendia et al [3] showed that the addition of a small volume fraction of MWCNT in 3YTZP sintered under specific SPS conditions leads to a balance between ageing and crack resistance never reached before. Following this line, it should be interesting to give some arguments on the balance between LTD and toughness achieved in SWNT/3YTZP composites. Regarding the fracture toughness values, Vickers

indentation technique was used in our previous works [16] and [34] to compare the fracture toughness of some of the composites studied in the current research. Although the K_{IC} values obtained from Vickers indentations are not fully quantitative and therefore are not directly comparable to the values in the literature for CNT-ceramic matrix materials tested with the SENB method, it is well accepted to use them to compare different compositions tested in a same study or for comparison purpose with previous works. For the composites with low SWNT (up to 2 vol%) content prepared using UP dispersion [34], the obtained K_{IC} data followed a increasing trend for the composites with increasing SWNT vol%. This slight enhancement was related to CNT toughening mechanisms present in the composites (such as CNT crack bridging and pull out, and CNT ropes debundling and uncoiling). Increasing K_{IC} values with SWNT content were also found for higher SWNT content 3YTZP composites prepared using UB dispersion (C2.5-UB, C5-UB and C10-UB composites) in [16]. In view of the results of the current work, an increase of K_{IC} should be also expected as the stability of tetragonal zirconia (more proneness to phase transformation) is decreased with increasing SWNT content at the grain boundaries. Given the better resistance to aging of the SWNT/3YTZP composites, the improvement observed also in K_{IC} values [16, 34] involves a step forward in the trade-off between crack resistance and aging in the 3YTZP system.

5. CONCLUSIONS

For the processing conditions used in this work, it is shown than the incorporation of carbon nanotubes finely dispersed at the zirconia grain boundaries decreases the stability of the tetragonal phase at room temperature in the as–sintered samples by modifying the stiffness and the matrix effect.

The increased percolation degree of the SWNT bundles network in the SWNT/3YTZP composites increases the monoclinic content in the as–sintered samples while avoiding extensive cracking. The presence of these nanostructures at the grain boundaries, which can absorb the elastic energy related to the martensitic transformation by SWNTs bending and inter–bundle sliding, is pointed out as responsible for the reduced micro–cracking of the composites.

The addition of a small content (0.5–2.5 vol%) of SWNT in a 3YTZP matrix results in a material exhibiting an improved LTD resistance. As the carbon nanotube incorporation modifies the ceramic grain boundaries and at least partly because they do resist more micro-cracking, the resistance to aging is increased substantially.

6. AKNOWLEDGEMENTS

This work has been supported by the Ministerio de Economía y Competitividad (Spanish Government) through project MAT2015–67889–P, cofunded by European FEDER fundings, and by the Junta de Andalucía (Andalusian Government) through project P12–FQM–1079. XRD and microscopy studies have been performed in CITIUS 54 facilities (Universidad de Sevilla). The authors would also like to acknowledge Dr. S. Medina Carrasco for his kind help and advice in the analysis of the XRD results (X Ray Laboratory, CITIUS) and Ms. C. González Orellana for her experimental support in aging tests.

7. REFERENCES

[1] J. Chevalier, L. Gremillard, A.V. Virkar, D.R. Clarke, The Tetragonal–Monoclinic Transformation in Zirconia: Lessons Learned and Future Trends, J. Am. Ceram. Soc. 92

(2009) 1901–1920.

[2] R.C. Garvie, R.H.J. Hannink, R.T. Pascoe, Ceramic Steel, Nature 258 (1975) 703–704.

[3] N. Garmendia, S. Grandjean, J. Chevalier, L.A. Diaz, R. Torrecillas, I. Obieta, Zirconia–multiwall carbon nanotubes dense nano–composites with an unusual balance between crack and ageing resistance, J. Eur. Ceram. Soc. 31 (2011) 1009–1014.

[4] L. Ruiz, M.J. Ready, Effect of heat treatment on grain size. Phase assemblage, and mechanical properties of 3-mol%Y-TZP, J. Am. Ceram. Soc. 79 (1996) 2331-2340.

[5] P.F. Becher, M. V. Swain, Grain-size-dependent transformation behavior in polycrystalline tetragonal zirconia, J. Am. Ceram. Soc. 75 (1992) 493-502.

[6] T. Sakuma, H. Eda, H. Sato, Science and technology of zirconia III edited by S. Somiya, N. Yamamoto, H. Yanagida. Adv. Ceram. 24A (1988) 357-363.

[7] T. Masaki, K. Sinjo, Mechanical properties of highly toughened ZrO_2-Y_2O_3, Ceram. Int. 13 (1987) 109-112.

[8] L. Gao, T.S. Yen, J.K. Guo, Science and technology of zirconia III edited by S. Somiya, N. Yamamoto, H. Yanagida. Adv. Ceram. 24A (1988) 405-414.

[9] F.F. Lange, D.J. Green, Advances in Ceramics 3 edited by A.H. Heuer, L.W. Hobbs (1981) 217-225.

[10] O. Vasylkiv, Y. Sakka, V.V. Skorokhod, Low-temperature processing and mechanical properties of zirconia and zirconia-alumina nanoceramics, J. Am. Ceram. Soc. 86 (2003) 299-304.

[11] B. Basu, Toughening of yttria-stabilised tetragonal zirconia ceramics, Int. Mater. Rev. 50 (2005) 239–256.

[12] F. Zhang, J. Chevalier, C. Olagnon, M. Batuk, J. Hadermann, B. Van Meerbeek, J. Vleugels, Grain-boundary engineering for aging and slow-crack-growth resistant zirconia, J. Dent. Res. 96 (2017) 774–779.

[13] N.P. Padture, Multifunctional Composites of Ceramics and Single–Walled Carbon Nanotubes, Adv. Mater. 21 (2009) 1767–1770.

[14] T.Y. Luo, T.X. Liang, C.S. Li, Stabilization of cubic zirconia by carbon nanotubes, Mater. Sci. Eng. A366 (2004) 206–209.

[15] S. Rani, M. Kumar, S. Sharma, D. Kumar, Role of graphene in structural transformation of zirconium oxide, J. Sol–Gel Sci. Technol. 71 (2014) 470–476.

[16] R. Poyato, A. Gallardo–López, F. Gutiérrez–Mora, A. Morales–Rodríguez, A. Muñoz, A. Domínguez–Rodríguez, Effect of high SWNT content on the room temperature mechanical properties of fully dense 3YTZP/SWNT composites, J. Eur. Ceram. Soc. 34 (2014) 1571–1579.

[17] M.H. Bocanegra–Bernal, A. Reyes–Rojas, A. Aguilar–Elguézabal, E. Torres–Moye, J. Echeberria, X–ray diffraction evidence of a phase transformation in zirconia by the presence of graphite and carbon nanotubes in zirconia toughened alumina composites, Int. Journal of Refractory Metals and Hard Materials 35 (2012) 315–318.

[18] S. Shimada, Microstructural observation of ZrO_2 scales formed by oxidation of ZrC single crystals with formation of carbon, Solid State Ionics 101–103 (1997) 749–753.

[19] D.N. Wang, K.M. Liang, The effect of carbon on the phase stability of zirconia, J. Mater. Sci. Letters 17 (1998) 343–44.

[20] R. Poyato, J. Macías–Delgado, A. Gallardo–López, A. Muñoz, A. Domínguez–Rodríguez, Microstructure and impedance spectroscopy of 3YTZP/SWNT ceramic nanocomposites, Ceram. Int. 41 (2015) 12861–12868.

[21] A. Kasperski, A. Weibel, D. Alkattan, C. Estournès, Ch. Laurent, A. Peigney, Double–walled carbon nanotube/zirconia composites: Preparation by spark plasma sintering, electrical conductivity and mechanical properties, Ceram. Int. 41 (2015) 13731–13738.

[22] J.P. Zhou, Q.M. Gong, K.Y. Yuan, J.J Wu, Y.F. Chen, C.S. Li, J. Liang, The effects of multiwalled carbon nanotubes on the hot–pressed 3 mol% yttria stabilized zirconia ceramics, Mater. Sci. Eng. A 520 (2009) 153–157.

[23] M. Mazaheri, D. Mari, Z.R. Hesabi, R. Schaller, G. Fantozzi, Multi–walled carbon nanotube/nanostructured zirconia composites: Outstanding mechanical properties in a wide range of temperature, Comp. Sci. Tech. 71 (2011) 939–945.

[24] J.H. Shin, S.H. Hong, Microstructure and mechanical properties of single wall carbon nanotube reinforced yttria stabilized zirconia ceramics, Mater. Sci. Eng. A 556 (2012) 382–387.

[25] L. Shen, Y.H. Han, C. Xiang, H. Tang, A. Mukherjee, S. Kim, S.I. Bae, Q. Huang, Phase transformation behavior of ZrO_2 by addition of carbon nanotubes consolidated by spark plasma sintering, Scripta Mater. 69 (2013) 736–739.

[26] P. Mohapatra, S. Rawat, N. Mahato, K. Balani, Restriction of Phase Transformation in Carbon Nanotube–Reinforced Yttria–Stabilized Zirconia, Metall. Mater. Trans. A 46A (2015) 2965–2974.

[27] L. Melk, J.J. Roa Rovira, F. García–Marro, M.L. Antti, B. Milsom, M.J. Reece, M. Anglada, Nanoindentation and fracture toughness of nanostructured zirconia/multi–walled carbon nanotube composites, Ceram. Int. 41 (2015) 2453–2461.

[28] R. Poyato, A.L. Vasiliev, N.P. Padture, H. Tanaka, T. Nishimura, Aqueous colloidal processing of single–wall carbon nanotubes and their composites with ceramics, Nanotech. 17 (2006) 1770–1777.

[29] A. Gallardo–López, A. Morales–Rodríguez, J. Vega–Padillo, R. Poyato, A. Muñoz, A. Domínguez–Rodríguez, Enhanced carbon nanotube dispersion in 3YTZP/SWNTs composites and its effect on room temperature mechanical and electrical properties, J. All. Comp. 682 (2016) 70–79.

[30] J.M. Valverde, S. Medina, Crystallographic transformation of limestone during calcinations under CO_2, Phys. Chem. Chem. Phys. 17 (2015) 21912–21926.

[31] The Rietveld Method, in: R.A. Young (Ed.), IUCr Monographs on Crystallography No.5, Oxford University Press, New York, 1993.

[32] A. Bruker, TOPAS 5 user manual, Bruker AXS GmbH, Germany Search PubMed, Karlsruhe, 2014.

[33] ISO 13356: Implants for surgery - Ceramic materials based on yttria-stabilized tetragonal zirconia (Y-TZP) (1997).

[34] R. Poyato, J. Macías–Delgado, A. García–Valenzuela, Á. Gallardo–López, A. Morales–Rodríguez, A. Muñoz, A. Domínguez–Rodríguez, Mechanical and electrical properties of low SWNT content 3YTZP composites, J. Eur. Ceram. Soc. 35 (2015) 2351–2359.

[35] A. Morales–Rodríguez, Á. Gallardo–López, A. Fernández–Serrano, R. Poyato, A. Muñoz, A. Domínguez–Rodríguez, Improvement of Vickers hardness measurement on SWNT/Al_2O_3 composites consolidated by spark plasma sintering, J. Eur. Ceram. Soc. 34 (2014) 3801–3809.

[36] M. Estili, Y. Sakka, Recent advances in understanding the reinforcing ability and mechanism of carbon nanotubes in ceramic matrix composites, Sci. Technol. Adv. Mater. 15 (2014) 064902.

[37] G. Yamamoto, Y. Sato, T. Takahashi, M. Omori, T. Hashida, A. Okubo, K. Tohji, Single–walled carbon nanotube–derived novel structural material, J. Mater. Res. 21 (2006)1537–1542.

[38] E. Mohamed, M. Taheri, M. Mehrjoo, M. Mazaheri, A.M. Zahedi, M.A. Shokrgozar, F. Golestani–Fard, In vitro biocompatibility and ageing of 3YTZP/CNTs composites, Ceram. Int. 41 (2015) 12773–12781.

FIGURE CAPTIONS

Figure 1. SEM micrographs illustrating the SWNT distribution within the 3YTZP matrix in the as–sintered SWNT/3YTZP composites: (A,B) C1.5–UP and (C,D) C1.5– UB, respectively. Low–magnification BSE images of polished cross–sections are presented on the left and high–resolution SEM fracture surfaces on the right side. Agglomerates are pointed by arrows in (C).

Figure 2. A) XRD patterns of polished surfaces of the as–sintered SWNT/3YTZP composites. XRD patterns of the 3YTZP powder and the monolithic 3YTZP ceramic are also included for comparison. B) Enlarged view of the 2θ–angle range between 28º and 32º for the XRD pattern of C0.5–UP compared with the corresponding ones for the powder and the monolithic zirconia ceramic.

Figure 3. Profile–fitting patterns of the as–sintered monolithic 3YTZP ceramic: experimental and calculated profile intensities along with their difference on the same scale.

Figure 4. Monoclinic ZrO_2 weight fraction *vs.* GB–SWNT content measured for the as–sintered SWNT/3YTZP composites. The value for the monolithic 3YTZP ceramic is also included for comparison.

Figure 5. Surface phase transformation curves for the monolithic 3YTZP and C0.5–UP after hydrothermal aging experiments. The monoclinic contents for the C2.5–UP composite after 10 and 50 h hydrothermal aging times are also presented.

Figure 6. Cross–section SEM micrograph of the monolithic 3YTZP after 10 h hydrothermal degradation test. The inset shows a magnified view of the zone close to the surface exposed to water.

Tables

Table I. Relative density, microstructural features –SWNT content at grain boundaries and ceramic grain size (mean value and standard deviation)– and electrical conductivity of the as–sintered SWNT/3YTZP composites. Data corresponding to the monolithic 3YTZP ceramic sintered under the same conditions as well as C5–UB and C10–UB from ref. [7] are also included for comparison.

Sample	Nominal SWNTs (vol%)	GB–SWNTs (vol%)	ρ_r (%)	<d> ± sd (nm)	σ_e (10^{-2} S m^{-1})
3YTZP	0	0	100	220 ± 90 [a]	Insulating
C0.5–UP	0.5	0.5	98.5	240 ± 80 [b]	Insulating
C1.5–UP	1.5	1.5	99.5	220 ± 80 [b]	2.8 [b]
C2.5–UP	2.5	2.5	100	230 ± 100	20.7
C0.5–UB	0.5	0.32 [a]	100	230 ± 80 [a]	Insulating [a]
C1.5–UB	1.5	1.10 [a]	99.4	240 ± 80 [a]	0.06 [a]
C5–UB	5	2.6	99.3	190 ± 80 [c]	Conductor
C10–UB	10	7.9	100	240 ± 130 [c]	Conductor

[a] From ref. [24]. [b] From ref. [11]. [c] From ref. [7].

Table II. Crystallographic phase quantification (cubic, tetragonal and monoclinic zirconia content) obtained from Rietveld refinement of XRD profiles shown in figure 2. Least significant digit of estimated standard deviation values are given in parentheses. The values of goodness–of–fit parameter and overall residual factors R_{wp} and R_{Bragg} for cubic, tetragonal and monoclinic phases obtained in our analysis are also given.

Sample	c–ZrO_2 (wt%)	t–ZrO_2 (wt%)	m–ZrO_2 (wt%)	GOF	R_{wp}	R_{Bragg}		
						c	t	m
Powder	5.0(2)	60.1(2)	35.0(2)	1.86	4.09	0.83	1.50	1.19
3YTZP	9.3(2)	86.0(3)	4.8(2)	2.80	6.12	1.47	1.66	1.43
C0.5–UB	12.2(2)	82.9(3)	4.8(2)	2.92	6.55	2.05	1.45	1.48
C0.5–UP	13.0(4)	81.3(4)	5.7(2)	2.17	4.79	0.47	1.18	1.21
C1.5–UB	10.8(2)	83.2(3)	6.1(2)	2.72	6.17	2.21	1.36	1.26
C1.5–UP	11.6(3)	80.0(4)	8.4(3)	2.79	6.25	1.41	1.59	1.70
C2.5–UP	12.3(3)	78.2(4)	9.4(2)	2.22	5.41	0.81	1.09	0.96
C5–UB [a]	-	74.3(9)	13.0(5)	1.24	6.47	0.65	1.27	2.26
C10–UB [a]	-	74.7(7)	19.0(4)	1.22	6.31	1.47	1.00	1.62

[a] Data corresponding to C5–UB and C10–UB estimated by Rietveld refinement of the X–ray diffractograms published in reference [7] are also included for comparison.

Figure 1

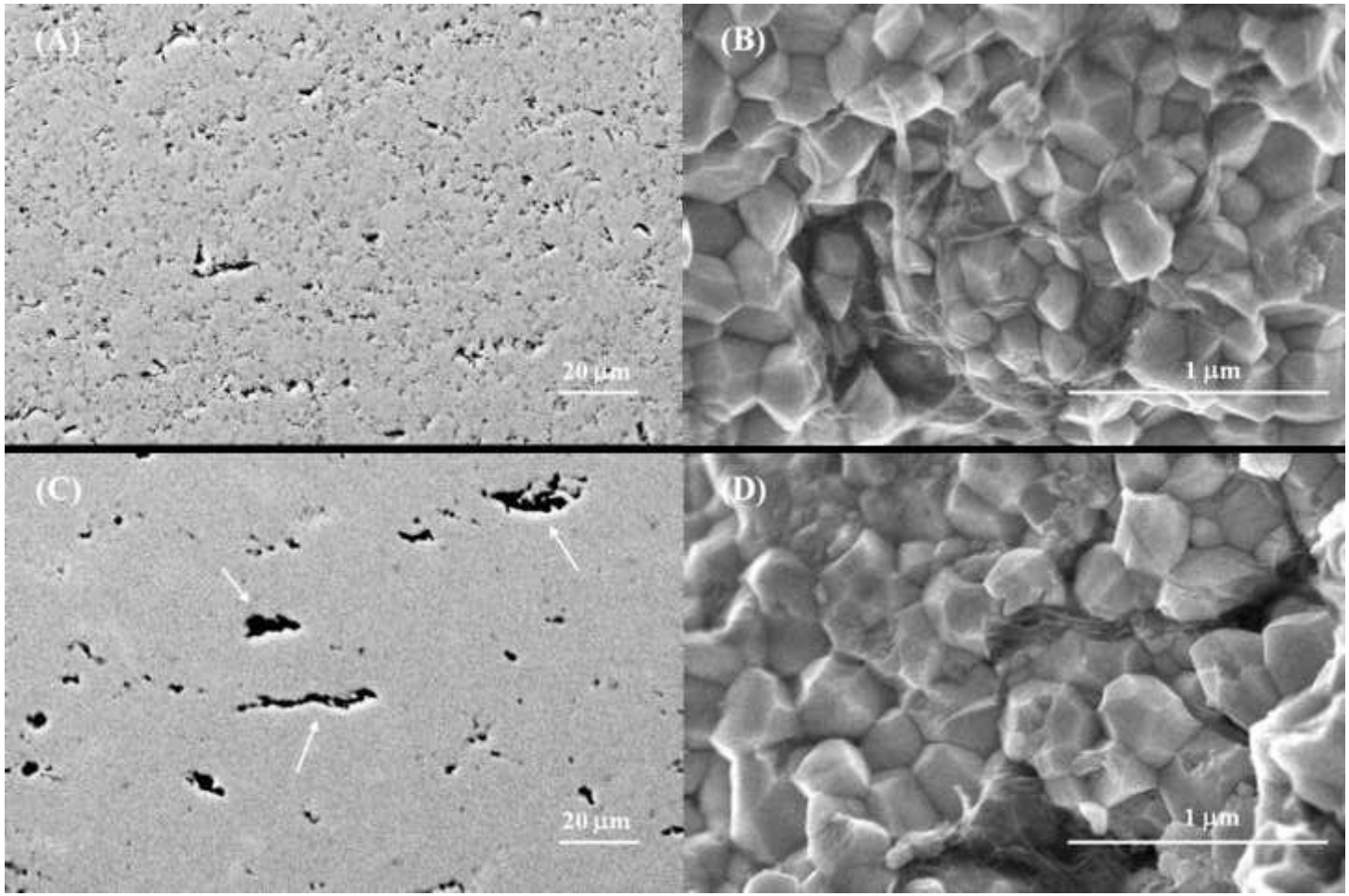

Figure 2

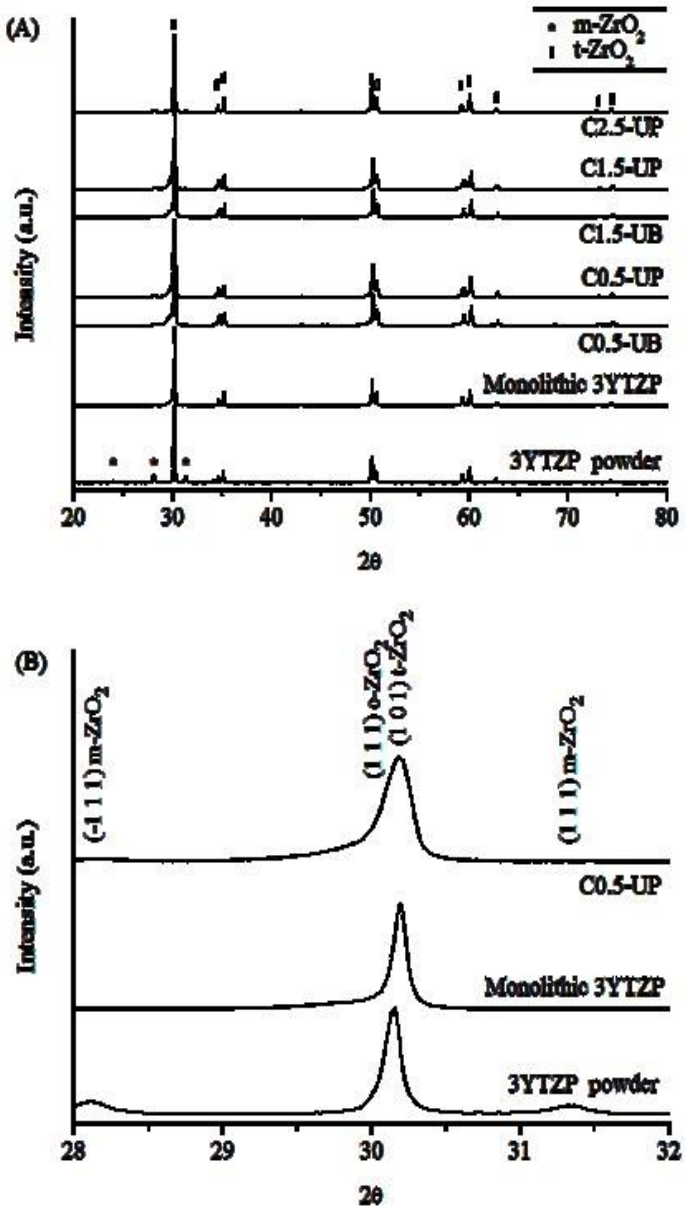
(A)
m-ZrO2
t-ZrO2
C2.5-UP
C1.5-UP
C1.5-UB
C0.5-UP
C0.5-UB
Monolithic 3YTZP
3YTZP powder
Intensity (a.u.)
20
30
40
50
60
70
80
2θ
(B)
(-1 1 1) m-ZrO2
(1 1 1) c-ZrO2
(1 0 1) t-ZrO2
(1 1 1) m-ZrO2
C0.5-UP
Monolithic 3YTZP
3YTZP powder
Intensity (a.u.)
28
29
30
31
32
2θ

Figure 3

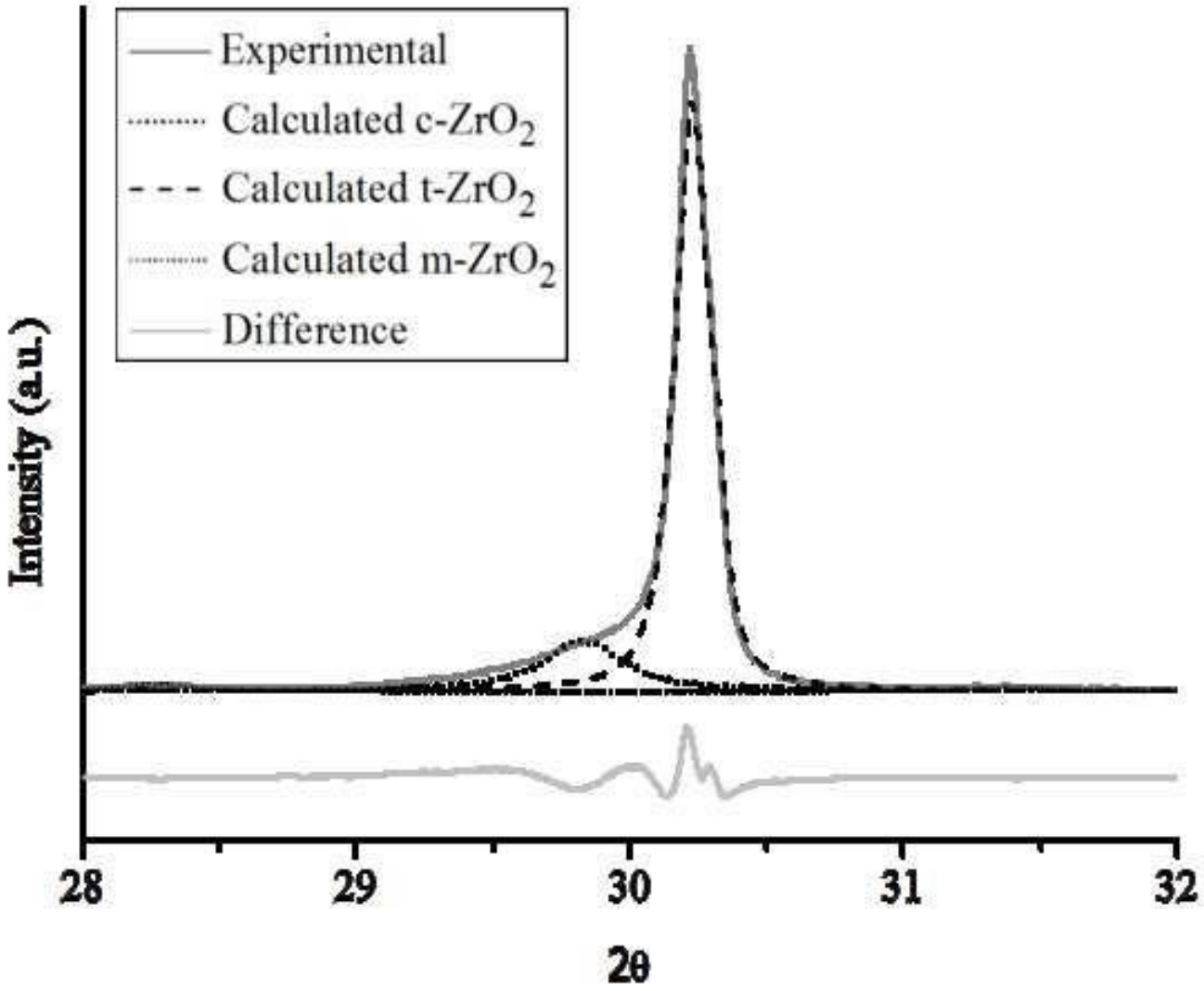
Experimental
Calculated c-ZrO2
Calculated t-ZrO2
Calculated m-ZrO2
Difference
Intensity (a.u.)
28
29
30
31
32
2θ

Figure 4

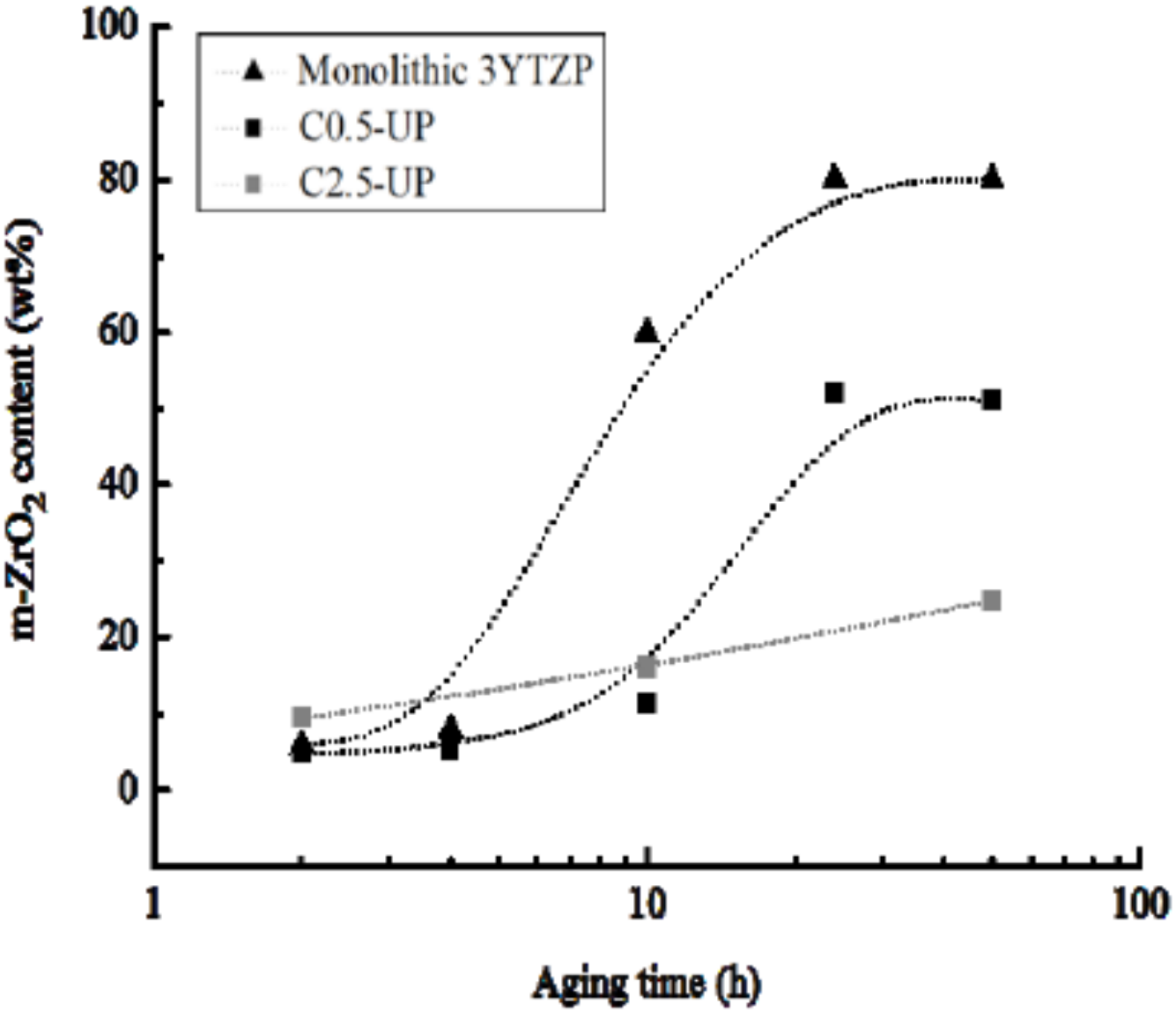
Monolithic 3YTZP
C0.5-UP
C2.5-UP
m-ZrO2 content (wt%)
100
80
60
40
20
0
1
10
100
Aging time (h)

Figure 5

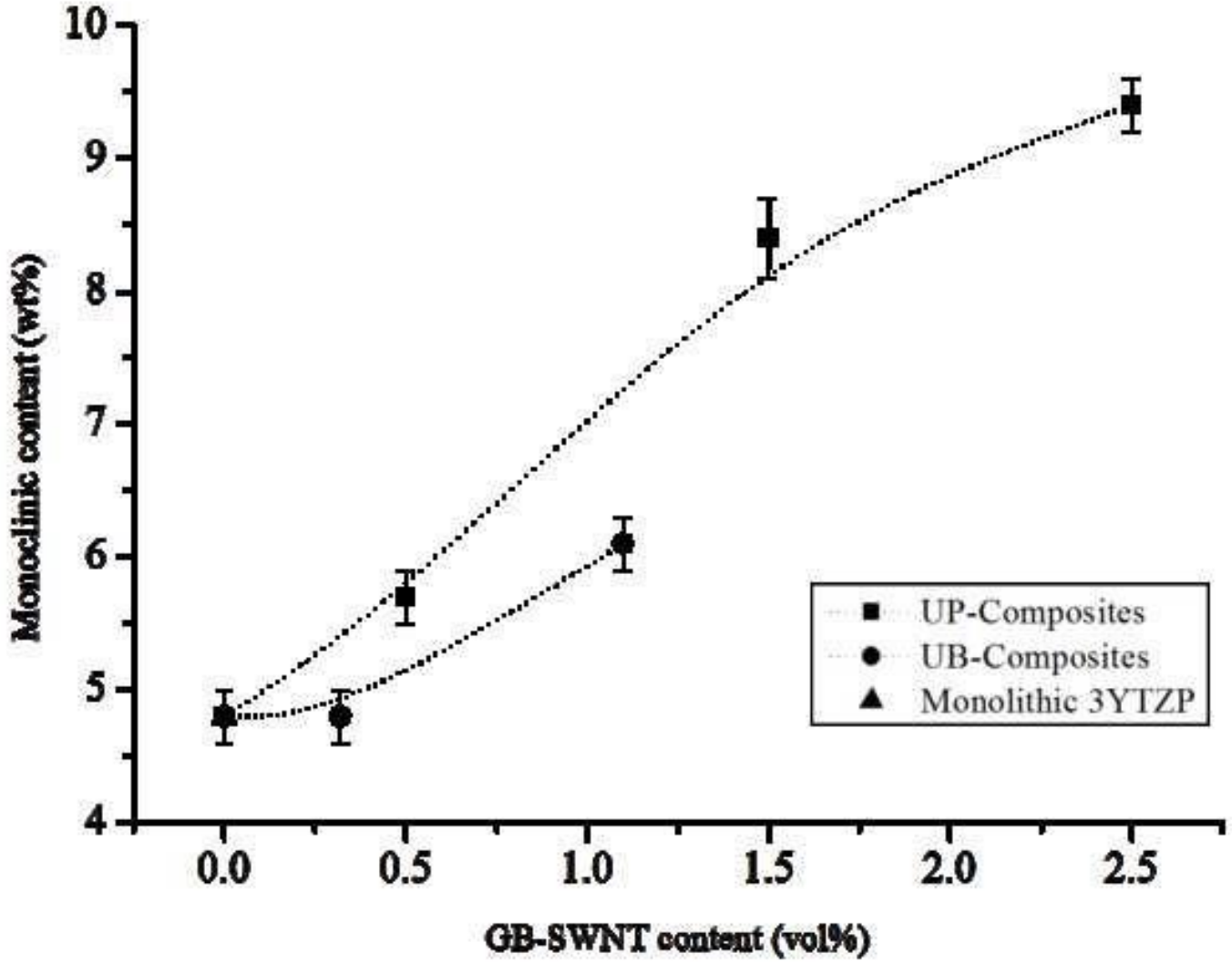
Monoclinic content (wt%)
10
9
8
7
6
5
4
0.0
0.5
1.0
1.5
2.0
2.5
GB-SWNT content (vol%)
UP-Composites
UB-Composites
Monolithic 3YTZP

Figure 6